

# Anomalous Behaviors of Visible Luminescence from Graphene Quantum Dots: Interplay between Size and Shape

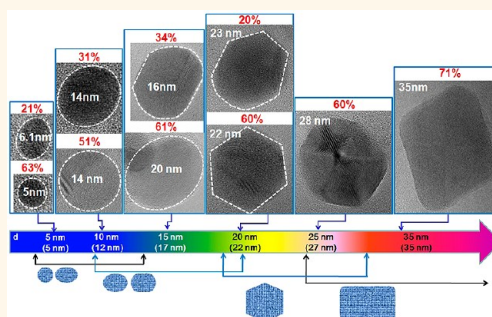
Sung Kim,<sup>†,‡</sup> Sung Won Hwang,<sup>‡,§</sup> Min-Kook Kim,<sup>§</sup> Dong Yeol Shin,<sup>†</sup> Dong Hee Shin,<sup>†</sup> Chang Oh Kim,<sup>†</sup> Seung Bum Yang,<sup>†</sup> Jae Hee Park,<sup>†</sup> Euyheon Hwang,<sup>†</sup> Suk-Ho Choi,<sup>†,\*</sup> Geunwoo Ko,<sup>‡</sup> Sunghyun Sim,<sup>‡</sup> Cheolsoo Sone,<sup>‡</sup> Hyoung Joon Choi,<sup>§</sup> Sukang Bae,<sup>⊥</sup> and Byung Hee Hong<sup>⊥</sup>

<sup>†</sup>Department of Applied Physics, Kyung Hee University, Yongin 446-701, Korea, <sup>‡</sup>Advanced Development Department, Samsung Electronics Co., Ltd, Yongin 446-711, Korea, <sup>§</sup>Department of Physics and IPAP, Yonsei University, Seoul 120-749, Korea, and <sup>⊥</sup>Department of Chemistry, SKKU Advanced Institute of Nanotechnology, Sungkyunkwan University, Suwon 440-746, Korea. \*These authors contributed equally to this work.

Recently, the quantum confinement effect (QCE) at a nanometer scale as in graphene quantum dots (GQDs) and graphene nanoribbons (GNRs) has attracted strong attention as one of the central issues in graphene-based electronics<sup>1–4</sup> because they provide the opportunity to explore novel structural, optical, and electrical phenomena not obtainable in other materials. Having a controllable nanometer-sized graphene system that can produce tunable light in the visible range is highly desirable for optoelectronic device applications of graphene. Therefore, it is essential to be able to engineer the bandgap of GQDs or GNRs by varying their size or width, respectively. Graphene is a single atomic layer of graphite with an infinite exciton Bohr radius due to its linear energy dispersion relation of the charge carriers,<sup>2,5</sup> resulting in QCE for graphene of any finite size.<sup>1,4</sup> The energy gap of GQDs falls off as approximately  $1/L$ ,<sup>4,6</sup> where  $L$  is the average size of GQDs. The bandgap has been observed up to  $\sim 0.4$  eV in GNRs,<sup>4,7</sup> while it can be controlled up to  $\sim 3$  eV in GQDs by reducing their size,<sup>6,8,9</sup> more promising for photonic nanodevices.

Near-ultraviolet-to-blue photoluminescence (PL) observed from GQDs fabricated through various processes<sup>8,10,11</sup> has been attributed to the recombination of electron–hole pairs in quantum-confined GQDs. However, the optical transitions for PL are allowed to be up to  $\sim 3$  eV in GQDs larger than  $\sim 3$  nm in size<sup>8,11,12</sup> and their size dependence is unclear,<sup>13</sup> not consistent with theoretically predicted bandgap energies of GQDs that well follow QCE but are not beyond 1 eV in these sizes.<sup>6,9</sup> Here, we report novel behaviors of absorption and

## ABSTRACT



For the application of graphene quantum dots (GQDs) to optoelectronic nanodevices, it is of critical importance to understand the mechanisms which result in novel phenomena of their light absorption/emission. Here, we present size-dependent shape/edge-state variations of GQDs and visible photoluminescence (PL) showing anomalous size dependences. With varying the average size ( $d_a$ ) of GQDs from 5 to 35 nm, the peak energy of the absorption spectra monotonically decreases, while that of the visible PL spectra unusually shows nonmonotonic behaviors having a minimum at  $d_a = \sim 17$  nm. The PL behaviors can be attributed to the novel feature of GQDs, that is, the circular-to-polygonal-shape and corresponding edge-state variations of GQDs at  $d_a = \sim 17$  nm as the GQD size increases, as demonstrated by high-resolution transmission electron microscopy.

**KEYWORDS:** graphene · quantum dot · size · shape · edge · photoluminescence

nonmonotonic visible PL of GQDs in the size range from 5 to 35 nm, and show that the anomalous PL phenomena can be explained by the size-dependent shape and corresponding edge-state variations of GQDs, as confirmed by high-resolution transmission electron microscopy (HRTEM).

## RESULTS AND DISCUSSION

We prepared GQDs by hydrothermal (chemical) cutting<sup>8</sup> of graphene sheets that

\* Address correspondence to sukho@khu.ac.kr.

Received for review June 28, 2012 and accepted August 10, 2012.

Published online August 11, 2012  
10.1021/nn302878r

© 2012 American Chemical Society

were obtained by thermal deoxidization of graphene oxide sheets made from natural graphite powder by a modified Hummers method.<sup>14,15</sup> GQDs at a particular size ( $d$ ) were obtained by filtering and dialysis processes. HRTEM images were obtained for six kinds of samples with  $d$  from 5 to 35 nm. Figure 1a shows a typical distribution of GQDs at  $d = 10$  nm (average size = 12 nm). Average size ( $d_a$ ) is defined as half of (width + length)

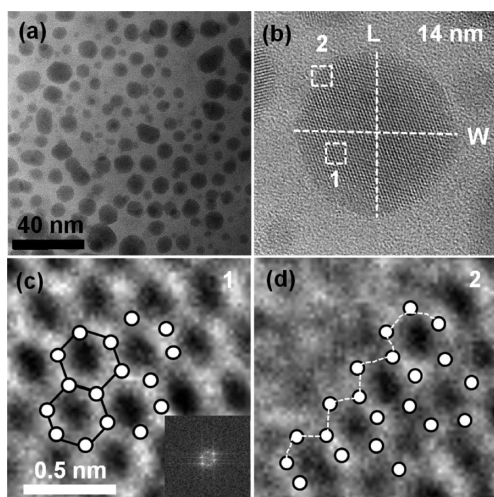


**Figure 1.** (a) A typical distribution of GQDs with an average size of 12 nm. (b) Definition of the average size: half of (width + length) of a GQD. (c) A magnified HRTEM image showing arrangements of carbon atoms in a typical circular GQD, which shows an average C–C bond length is 1.44 Å. (d) A magnified HRTEM image showing the edge of a typical circular GQD is of zigzag type.

of a GQD, as shown in Figure 1b. It is possible to see the hexagonal unit cell of GQDs in higher-resolved HRTEM images, as shown for a typical circular GQD in Figure 1c, demonstrating that the GQDs consist of graphene. The average C–C bond length is estimated to be about 1.44 Å, very close to that in graphite.<sup>16</sup> Figure 1d shows that the edge of a typical circular GQD is of zigzag type.

The HRTEM images were analyzed for individual GQDs to classify their major shapes at each  $d$ . Figure 2 shows the most common shapes for a given size of GQDs in percentage ( $p$ ) (see also Supporting Information Figure S1). Average sizes of GQDs estimated from the HRTEM images at each  $d$  are indicated in parentheses at the bottom of Figure 2. Circular and elliptical GQDs of  $\sim 5$  and  $\sim 12$  nm average sizes are produced at  $d = 5$  and 10 nm, respectively. In these samples, circular GQDs occupy more than 50% of the total number of GQDs at each  $d$ . At  $d = 15$  nm, circular GQDs disappear and only elliptical GQDs are seen with  $\sim 1/3$  of them deformed. At  $d = 20$  nm, most GQDs are hexagon-shaped, but  $\sim 1/4$  of them are deformed with curved sides. At  $d = 25$  nm, the major portion of GQDs are still hexagon-shaped with minor irregular-shaped GQDs. At  $d = 35$  nm, most QDs are shaped as parallelogram-type rectangles with rounded vertices. Recently, it has been known that the equilibrium shape of the GQDs synthesized by transformation of  $C_{60}$  can be tailored by optimizing the annealing temperature and the density of the carbon clusters.<sup>17</sup>

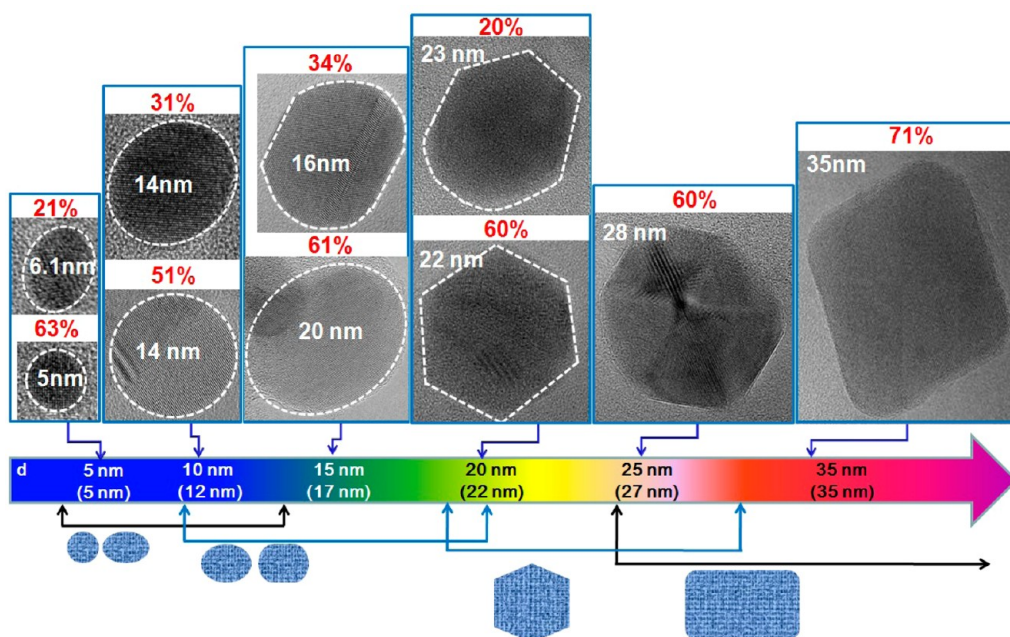


**Figure 2.** HRTEM images of GQDs for their major shapes and corresponding populations ( $p$ ) with increasing average size of GQDs. Here, the dotted line indicates the region of a GQD and  $p$  is defined as the ratio of number of GQDs with a major shape at each average size. Average sizes ( $d_a$ ) of GQDs estimated from the HRTEM images at each  $d$  are indicated in the parentheses at the bottom of Figure 2. The connected arrows indicate the range of the average size in which GQDs with particular major shapes are found.

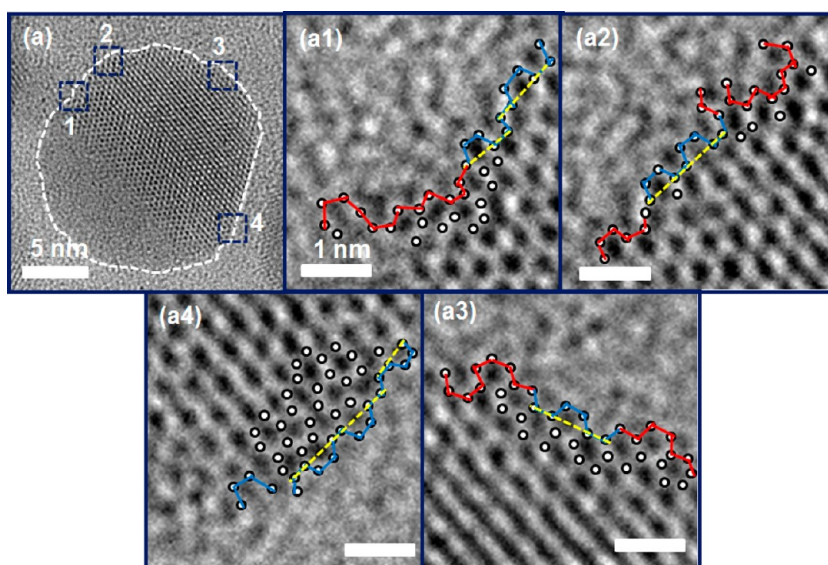


**Figure 3.** A HRTEM image showing mixed edges of zigzag and armchair at four different edge positions (1–4) of a typical GQD (a) with partially curved and linear regions at the edge. Red and blue lines show zigzag and armchair edges, respectively, in the magnified HRTEM images (a1–a4) corresponding to the four edge positions. Zigzag and armchair edges are mixed in curved regions, but the armchair edge is dominant in linear regions. The scale bars in a1–a4 are all 1 nm.

The detailed analysis of HRTEM images for GQDs shows that the periphery of GQDs consists of mixed zigzag and armchair edges. Figure 3 shows the edge states at four different edge positions (1–4) of a typical GQD (a) with partially curved and linear regions at the edge. Red and blue lines show zigzag and armchair edges, respectively, in the magnified HRTEM images (a1–a4) corresponding to the four edge positions. We find that both edges are mixed in curved periphery while the armchair edge appears more frequently in straight periphery. As a consequence, it appears that circular/elliptical GQDs consist of both edges, but polygonal GQDs consist mostly of armchair edge.

Atomic force microscopy (AFM) images/height profiles of GQDs show that the average thickness of GQDs increases with increasing their size (see Supporting Information Figure S2). For  $d_a \leq 17$  nm, the GQDs consist mostly of 1–3 graphene layers, but for  $d_a \geq 22$  nm, the GQDs comprising more than 5 graphene layers are also found. These results are consistent with the electron energy loss spectroscopy (EELS) results (see Supporting Information, Figure S3).

There have been several reports on the absorption spectra of graphene-related materials. For graphene oxide sheets, a typical absorption peak has been observed at 5.4 eV,<sup>8</sup> corresponding to the  $\pi \rightarrow \pi^*$  transition at M point of the Brillouin zone. It has been theoretically expected that with/without exciton effects, the interband transitions of a graphene sheet form a prominent absorption peak at 4.55 and 5.15 eV, respectively.<sup>18</sup> Blue-luminescent GQDs in water have been shown to exhibit absorption spectrum peaked at 3.9 eV.<sup>8</sup> For the GQDs in this work, however, the absorption peaks are observed at even larger energies.

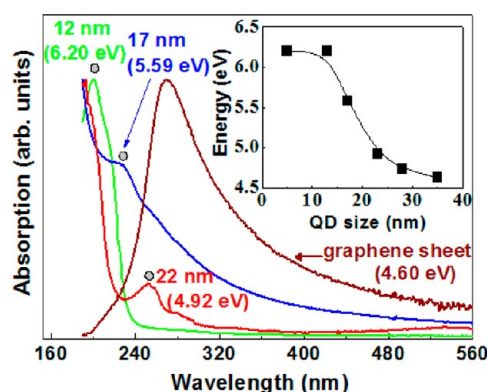


**Figure 4.** Absorption spectra for three typical GQDs of 12, 17, and 22 nm average sizes dispersed in DI water and a graphene sheet. Filled circular dots indicate the peak positions of the absorption spectra for GQDs. Inset: absorption peak energy as a function of average GQD size.

Figure 4 shows absorption spectra of different-size GQDs dispersed in deionized (DI) water and a graphene sheet (see also Supporting Information Figure S4). The absorption peak of GQDs is blue-shifted with respect to that of a graphene sheet (270 nm, 4.6 eV), and is sequentially shifted to higher energies by reducing their size, consistent with the QCE. The inset shows the peak energy as a function of  $d_a$ . As  $d_a$  increases from 5 to 35 nm, the peak energy almost monotonically decreases from  $\sim 6.2$  to  $\sim 4.6$  eV, very close to that of a graphene sheet.

Figure 5a shows size-dependent PL spectra excited at 325 nm for GQDs in DI water. The peak energy and the shape of the PL spectra are strongly dependent on the size of GQDs. A sharp PL peak at 365 nm originates from DI water<sup>19</sup> (see Supporting Information Figure

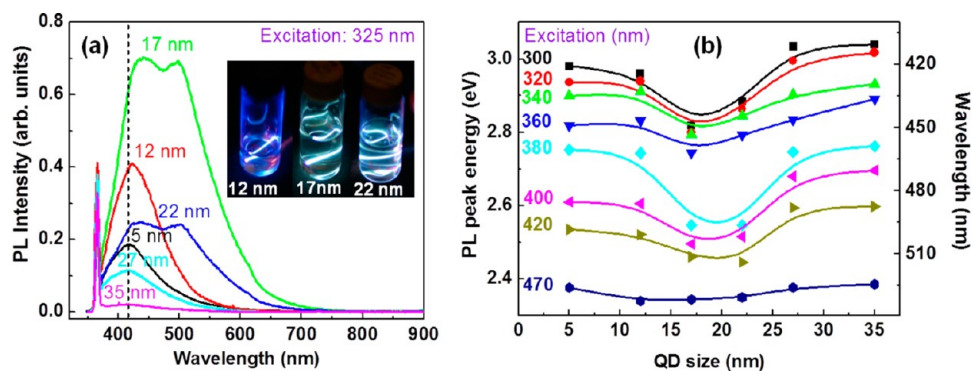


**Figure 5.** (a) Size-dependent PL spectra excited at 325 nm for GQDs of 5–35 nm average sizes in DI water. Inset: different colors of luminescence from GQDs depending on their average size for three typical GQDs of 12, 17, and 22 nm average sizes. (b) Dependence of PL peak shifts on the excitation wavelength from 300 to 470 nm for GQDs of 5–35 nm average sizes.

S5). The inset of Figure 5a shows different colors of luminescence depending on the size of GQDs. Especially for  $d_a = 17$  and 22 nm, the PL spectra are resolved in two PL bands, irrespective of the excitation wavelength, possibly resulting from combination of different-size/shape GQDs, as shown in Figure 2. As the excitation wavelength is changed from 300 to 470 nm, the PL peak sequentially shifts to longer wavelengths (see also Supporting Information Figure S5). This trend is similar for all GQD sizes. Figure 5b summarizes excitation-wavelength-dependent PL peak shifts for various-size GQDs. All PL spectra show similar size-dependent peak shifts, almost irrespective of excitation wavelength except 470 nm. The PL peak energy decreases as  $d_a$  increases up to  $\sim 17$  nm, consistent with the QCE. However, for  $d_a > \sim 17$  nm the PL peak energy increases with increasing  $d_a$ ; in other words, the QCE no longer holds. This unusual size dependence of luminescence is similar to what was found in reconstructed Si nanoparticles.<sup>20,21</sup>

It has been reported that after the hydrothermal treatment in the fabrication processes of GQDs, several oxygen-functional groups (OFGs) could remain at the edges of GQDs, thereby possibly affecting the PL behaviors of GQDs.<sup>8,13</sup> We studied the effect of the OFGs such as C–O, C=O, and COOH on the structure of GQDs by X-ray photoelectron spectroscopy (XPS) for various-size GQDs. The XPS peaks resolved based on the previous report<sup>13</sup> did not give any evidence that the population of the OFGs relative to that of the C=C bond depends on the size of GQDs (see Supporting Information Figure S6). This suggests that despite the presence of the OFGs in GQDs, they do not give any size-dependent effect on the structures of GQDs, resulting in a negligible effect on the size-dependent PL behaviors of GQDs.

As shown in Figures 2 and 3, for  $d_a \leq \sim 17$  nm the majority of GQDs is of circular/elliptical shape with mixed edges of zigzag and armchair, but for  $d_a > \sim 17$  nm they are of polygonal shape mostly with armchair edge. The PL peak energy decreases as  $d_a$

increases as long as GQDs keep their shape circular/elliptical for  $d_a \leq \sim 17$  nm, but when the shape of GQDs varies into polygons for  $d_a > \sim 17$  nm, the PL peak energy increases with increasing  $d_a$ . These results suggest that the anomalous size dependence of the PL peak above  $d_a = \sim 17$  nm can be attributed to the novel feature of GQDs, that is, the circular-to-polygonal-shape and corresponding edge-state variations of GQDs at  $d_a = \sim 17$  nm as the GQD size increases. Our calculations also showed that the averaged PL energy could increase with increasing  $d_a$  (contradictory to QCE) due to the change of the shape or the edge type at larger  $d_a$ . (see Supporting Information Figure S7)

Several theoretical studies have shown that the bandgap energies of GQDs in the size range of 5–35 nm are not beyond  $\sim 1.0$  eV,<sup>6,9</sup> which cannot explain why the experimental PL peak energies of GQDs reach  $\sim 3$  eV, as shown in Figure 5 and as seen in previous reports.<sup>8,11,12</sup> The visible PL found in a graphene sheet has been explained by minimization of thermalization due to electron–phonon scattering by using ultrafast high-power light source<sup>22–24</sup> or by formation of excited-state relaxation channel resulting in inelastic light scattering by electric doping.<sup>25</sup> Our study shows that such light-emission phenomena can also be explored in GQDs because electronic transitions can be modified in nanometer-sized systems to produce strong visible PL emissions in a controlled fashion, that is, by size and size-dependent shape/edge-state variations of GQDs. The high-energy PL of GQDs is especially efficient due to the unique properties of graphene: fast carrier–carrier scattering dominating over electron–phonon scattering, predicted by theory,<sup>26,27</sup> and confirmed by ultrafast dynamics experiments.<sup>28,29</sup> This facilitates direct recombination of excited e–h pairs producing such high-energy PL before thermalization of the carriers with the lattice. The high Coulomb scattering rate of graphene,<sup>30–32</sup> which is attributed to the strongly reduced dielectric screening in the two-dimensional structure, is also

essential for producing high-density nonequilibrium carriers responsible for the strong e–h recombination.

## CONCLUSION

We successfully fabricated various-size GQDs and examined their structures with HRTEM, AFM, and EELS. We found that GQDs appeared as the circular shape with mixed edges of zigzag and armchair for  $d_a < \sim 17$ , but as the polygonal shape mostly with armchair edges for  $d_a \geq \sim 17$  nm. We also measured the size-dependent absorption and PL spectra of GQDs. As the size of GQDs increased, the absorption peak energy of

GQDs decreased, which could be explained by the QCE, but their PL peak energies unusually showed nonmonotonic behaviors having a minimum at  $d_a = \sim 17$  nm. On the basis of the HRTEM results, the anomalous PL behaviors were attributed to the size-dependent shape and corresponding edge variations of GQDs. In addition, the visible PL observed far beyond the band gap of GQDs was especially efficient due to the peculiar scattering mechanism of graphene, that is, fast carrier–carrier scattering dominating over electron–phonon scattering in graphene.

## EXPERIMENTAL SECTION

GQDs were fabricated by the following processes. Graphene oxide (GO) sheets were obtained from natural graphite powder by a modified Hummers method.<sup>14,15</sup> The GO sheets were subsequently deoxidized in a tube furnace at 250 °C for 2 h under Ar ambient to prepare reduced graphene oxide powder, 0.05 g of which were then oxidized in concentrated 10-mL H<sub>2</sub>SO<sub>4</sub> and 30-mL HNO<sub>3</sub> for 20 h under mild ultrasonication. The mixture was then diluted with 250-mL DI water and filtered through a 200-nm nanoporous membrane to remove the acids. The size-reduced/purified 0.2-g GO powder was redispersed in 40-mL DI water and the pH was tuned to 8 with NaOH. The suspension was transferred to a nitrogen-ambient furnace and heated at 250 °C for 10 h. After cooling to room temperature, the resulting powder was redispersed in 40-mL DI water for 2 h under ultrasonication. Then, by filtering the resulting suspension through a 200-nm nanoporous membrane, a brown filter solution was separated. Since the colloidal solution still contained some large graphene nanoparticles (<200 nm) emitting weak blue fluorescence, it was further filtered dialyzed in a dialysis bag of 3500 Da molecular weight overnight, thereby producing strongly fluorescent GQDs. The GQDs were separated as different sizes ( $d$ ) by using several dialysis bags of 1000–50000 Da and a 20-nm nanoporous membrane.

The morphologies of GQDs were analyzed using a transmission electron microscope (200 kV, JEM-2100F, Jeol Ltd., Japan) with EELS mapping capabilities. To make the HRTEM/EELS and AFM specimens the GQDs were dispersed in DI water, a drop of which was then put on a C- or SiO<sub>2</sub>-coated Cu grid (Tedpella, Inc.) and mica substrate, respectively. The topographic image and height profile of GQDs were obtained in a noncontact mode of AFM (Park System, model XE-100). Absorption spectra were measured using an Agilent 8453 UV–vis spectrophotometer. The excitation sources were  $\sim 40$  mW/cm<sup>2</sup> tungsten/deuterium lamps from which monochromatic light was selected using a grating monochromator and associated filters. PL spectra were measured at room temperature in a PTI's QuantaMaster 30 System with a 450 mW xenon arc lamp by varying the excitation wavelength. Emitted light was analyzed using a grating monochromator and a GaAs photomultiplier tube. All spectra were corrected for the spectral response of the instrument.

**Conflict of Interest:** The authors declare no competing financial interest.

**Acknowledgment.** This work was supported by National Research Foundation of Korea (NRF) grants funded by the Korea government (Ministry of Education, Science and Technology) (MEST), (No. 2011-0017373 and No. 2011-0014681). M.-K.K. and H.J.C. acknowledge support from NRF of Korea (Grant No. 2011-0018306). Computational resources were provided by KISTI Supercomputing Center (Project No. KSC-2011-C3-06).

**Supporting Information Available:** Additional information for the experimental results can be found in the Supporting Information section. This material is available free of charge via the Internet at <http://pubs.acs.org>.

## REFERENCES AND NOTES

- Ponomarenko, L. A.; Schedin, F.; Katsnelson, M. I.; Yang, R.; Hill, E. W.; Novoselov, K. S.; Geim, A. K. Chaotic Dirac Billiard in Graphene Quantum Dots. *Science* **2008**, *320*, 356–358.
- Geim, A. K.; Novoselov, K. S. The Rise of Graphene. *Nat. Mater.* **2007**, *6*, 183–191.
- Han, M. Y.; Özyilmaz, B.; Zhang, Y.; Kim, P. Energy Band-Gap Engineering of Graphene Nanoribbons. *Phys. Rev. Lett.* **2007**, *98*, 206805.
- Ritter, K. A.; Lyding, J. W. The Influence of Edge Structure on the Electronic Properties of Graphene Quantum Dots and Nanoribbons. *Nat. Mater.* **2009**, *8*, 235–242.
- Geim, A. K. Status and Prospects. *Science* **2009**, *324*, 1530–1534.
- Zhang, Z. Z.; Chang, K.; Peeters, F. M. Tuning of Energy Levels and Optical Properties of Graphene Quantum Dots. *Phys. Rev. B* **2008**, *77*, 235411.
- Son, Y.-W.; Cohen, M. L.; Louie, S. G. Energy Gaps in Graphene Nanoribbons. *Phys. Rev. Lett.* **2006**, *97*, 216803.
- Pan, D.; Zhang, J.; Li, Z.; Wu, M. Hydrothermal Route for Cutting Graphene Sheets into Blue-Luminescent Graphene Quantum Dots. *Adv. Mater.* **2010**, *22*, 734–738.
- Güçlü, A. D.; Potasz, P.; Hawrylak, P. Excitonic Absorption in Gate-Controlled Graphene Quantum Dots. *Phys. Rev. B* **2010**, *82*, 155445.
- Mueller, M. L.; Yan, X.; McGuire, J. A.; Li, L.-S. Triplet States and Electronic Relaxation in Photoexcited Graphene Quantum Dots. *Nano Lett.* **2010**, *10*, 2679–2682.
- Shen, J.; Zhu, Y.; Chen, C.; Yang, X.; Li, C. Facile Preparation and Upconversion Luminescence of Graphene Quantum Dots. *Chem. Commun.* **2011**, *47*, 2580–2582.
- Liu, R.; Wu, D.; Feng, X.; Müllen, K. Bottom-Up Fabrication of Photoluminescent Graphene Quantum Dots with Uniform Morphology. *J. Am. Chem. Soc.* **2011**, *133*, 15221–15223.
- Peng, J.; Gao, W.; Gupta, B. K.; Liu, Z.; Romero-Aburto, R.; Ge, L.; Song, L.; Alemany, L. B.; Zhan, X.; Gao, G.; *et al.* Graphene Quantum Dots Derived from Carbon Fibers. *Nano Lett.* **2012**, *12*, 844.
- Xu, Y.; Bai, H.; Lu, G.; Li, C.; Shi, G. Flexible Graphene Films via the Filtration of Water-Soluble Noncovalent Functionalized Graphene Sheets. *J. Am. Chem. Soc.* **2008**, *130*, 5856–5857.
- Pan, D.; Wang, S.; Zhao, B.; Wu, M.; Zhang, H.; Wang, Y.; Jiao, Z. Li Storage Properties of Disordered Graphene Nanosheets. *Chem. Mater.* **2009**, *21*, 3136–3142.
- Gass, M. H.; Bangert, U.; Bleloch, A. L.; Wang, P.; Nair, R. R.; Geim, A. K. Free-Standing Graphene at Atomic Resolution. *Nat. Nanotechnol.* **2008**, *3*, 676–681.
- Lu, J.; Yeo, P. S. E.; Gan, C. K.; Wu, P.; Loh, K. P. Transforming C<sub>60</sub> Molecules into Graphene Quantum Dots. *Nat. Nanotechnol.* **2011**, *6*, 247–252.
- Yang, L.; Deslippe, J.; Park, C.-H.; Cohen, M. L.; Louie, S. G. Excitonic Effects on the Optical Response of Graphene and Bilayer Graphene. *Phys. Rev. Lett.* **2009**, *103*, 186802.

19. Lobyshev, V. I.; Shikhinskaya, R. E.; Ryzhikov, B. D. Experimental Evidence for Intrinsic Luminescence of Water. *J. Mol. Liq.* **1999**, *82*, 73–81.
20. Wang, X.; Zhang, R. Q.; Lee, S. T.; Frauenheim, Th.; Niehaus, T. A. Anomalous Size Dependence of the Luminescence in Reconstructed Silicon Nanoparticles. *Appl. Phys. Lett.* **2008**, *93*, 243120.
21. Wang, X.; Zhang, R. Q.; Lee, S. T.; Niehaus, T. A.; Frauenheim, Th. Unusual Size Dependence of the Optical Emission Gap in Small Hydrogenated Silicon Nanoparticles. *Appl. Phys. Lett.* **2007**, *90*, 123116.
22. Liu, W.-T.; Wu, S. W.; Schuck, P. J.; Salmeron, M.; Shen, Y. R.; Wang, F. Nonlinear Broadband Photoluminescence of Graphene Induced by Femtosecond Laser Irradiation. *Phys. Rev. B* **2010**, *82*, 081408.
23. Lui, C. H.; Mak, K. F.; Shan, J.; Heinz, T. F. Ultrafast Photoluminescence from Graphene. *Phys. Rev. Lett.* **2010**, *105*, 127404.
24. Stoehr, R. J.; Kolesov, R.; Pflaum, J.; Wrachtrup, J. Fluorescence of Laser-Created Electron-Hole Plasma in Graphene. *Phys. Rev. B* **2010**, *82*, 121408.
25. Chen, C.-F.; Park, C.-H.; Boudouris, B. W.; Horng, J.; Geng, B.; Girit, C.; Zettl, A.; Crommie, M. F.; Segalman, R. A.; Louie, S. G.; *et al.* Controlling Inelastic Light Scattering Quantum Pathways in Graphene. *Nature* **2011**, *471*, 617–620.
26. Hwang, E. H.; Hu, B. Y. K.; Sarma, S. Inelastic Carrier Lifetime in Graphene. *Phys. Rev. B* **2007**, *76*, 115434.
27. Kim, R.; Perebeinos, V.; Avouris, P. Relaxation of Optically Excited Carriers in Graphene. *Phys. Rev. B* **2011**, *84*, 075449.
28. George, P. A.; Strait, J.; Dawlaty, J.; Shivaraman, S.; Chandrashekar, M.; Rana, F.; Spencer, M. G. Ultrafast Optical-Pump Terahertz-Probe Spectroscopy of the Carrier Relaxation and Recombination Dynamics in Epitaxial Graphene. *Nano Lett.* **2008**, *8*, 4248–4251.
29. Dawlaty, J. M.; Shivaraman, S.; Chandrashekar, M.; Rana, F.; Spencer, M. G. Measurement of Ultrafast Carrier Dynamics in Epitaxial Graphene. *Appl. Phys. Lett.* **2008**, *92*, 042116.
30. Rana, F. Electron-Hole Generation and Recombination Rates for Coulomb Scattering in Graphene. *Phys. Rev. B* **2007**, *76*, 155431.
31. Hwang, E. H.; Das Sarma, S. Dielectric Function, Screening, and Plasmons in Two-Dimensional Graphene. *Phys. Rev. B* **2007**, *75*, 205418.
32. Guinea, F. Charge Distribution and Screening in Layered Graphene Systems. *Phys. Rev. B* **2007**, *75*, 235433.